Available online at www.sciencedirect.com
ScienceDirect
Journal of Solid State Chemistry 180 (2007) 2478–2484
JOURNAL OF SOLID STATE CHEMISTRY
www.elsevier.com/locate/jssc

Thermal and photoluminescence properties of hydrated $YPO_4:Eu^{3+}$ nanowires

Weihua Di[a,b,*], Xiaoxia Zhao[a,b], Shaozhe Lu[a], Xiaojun Wang[a], Haifeng Zhao[a]

[a]*Key Laboratory of Excited State Physics, Changchun Institute of Optics, Fine Mechanics and Physics, Chinese Academy of Sciences, 16 Eastern South-Lake Road, Changchun 130033, People's Republic of China*
[b]*Graduate School of Chinese Academy of Sciences, Beijing 100039, People's Republic of China*

Received 27 December 2006; received in revised form 25 May 2007; accepted 11 June 2007
Available online 5 July 2007

Abstract

In this work, we used the solution precipitation route to synthesize Eu^{3+}-doped $YPO_4 \cdot nH_2O$ nanowires. The structure, morphology, composition, thermal behavior, and photoluminescence of as-synthesized product were characterized by X-ray diffraction (XRD), thermogravimetric and differential thermal analysis (TG/DTA), energy-dispersive X-ray spectroscopy (EDS), Fourier transform infrared spectroscopy (FT-IR), field emission scanning electron microscopic (FE-SEM) and photoluminescence (PL) spectra. The dependence of the structure, morphology, composition and luminescent properties on the thermal treatment was investigated. The results indicate that the aqueous synthesis has a better control on the structure, morphology, composition of the products, and that the heat treatment induces the transitions of the structure, composition, and luminescent properties.

Keywords: Rare earth; Yttrium orthophosphate; Hydrate; Luminescence; Thermal effect

1. Introduction

Nowadays, inorganic luminescent materials with nanometer dimensions have become an important field of modern nanoscale science and technology, which could find numerous potential applications in the fields of physics, chemistry and biology [1–5]. In particular, one-dimensional (1D) luminescent nanostructures have attracted considerable attention due to their potential applications as interconnectors and active components in fabricating the optoelectronic nanodevices [6,7].

Rare earth compounds have been widely used in high-performance luminescent devices, magnets, catalysts, and other functional materials owing to the numerous well-defined transition modes involving the 4*f* shell of their ions [8]. Recently, more and more interest has been focused on the synthesis and photoluminescence of rare earth compounds with nanosized scale for their potential application in optoelectronic devices and biological fluorescence labeling [9].

The aqueous synthesis including sol–gel, precipitation and hydrothermal method is commonly used to prepare the rare earth compound materials with nanosized scale [10,11]. The aqueous synthesis route may provide several adjustable synthetic parameters such as solution *p*H and concentration, and reaction time and temperature, thus the size, shape, morphology, and structure can be effectively controlled [12,13]. Several research groups used the hydrothermal method to synthesize rare earth compounds with different shapes and structures by changing the solution *p*H and temperature [14]. Jia et al. have successfully synthesized $LaVO_4$ nanocrystal with zircon-type structure using an ethylenediamine tetraacetic acid (EDTA) assisted hydrothermal method [12]. This structure cannot be obtained by conventional solid-state reaction. Generally, the luminescent nanocrystal synthesized by low-temperature aqueous route shows low crystallinity, numerous structural defects and surface adsorption of chemical

*Corresponding author. Key Laboratory of Excited State Physics, Changchun Institute of Optics, Fine Mechanics and Physics, Chinese Academy of Sciences, 16 Eastern South-Lake Road, Changchun 130033, People's Republic of China. Fax: +86 431 6176338.
E-mail address: weihdi@yahoo.com.cn (W. Di).

0022-4596/$ - see front matter © 2007 Elsevier Inc. All rights reserved.
doi:10.1016/j.jssc.2007.06.025

species, and low luminescent efficiency [7,15]. The thermal treatment at a suitable temperature is an alternative strategy to improve the crystallinity, surface, and luminescent efficiency [15]. In addition, the thermal treatment sometimes results in morphological variation, phase transition and structural transformation [15,16]. These changes can generally modify or improve the materials' properties. In this work, Eu^{3+}-doped $YPO_4 \cdot nH_2O$ nanowires were synthesized by solution precipitation method and the structure, morphology, and thermal and photoluminescence properties were characterized. The effects of thermal treatment on the structure, morphology and photoluminescence properties were investigated.

2. Experimental part

The samples were prepared by an aqueous precipitation method as follows. Appropriate amounts of high purity Y_2O_3 and Eu_2O_3 were dissolved in concentrated HNO_3 to form Y(III), Eu(III) solutions, respectively. Appropriate volume of $(NH_4)_2HPO_4$ solution was added slowly to above-mentioned lanthanide(III) solutions under vigorous stirring. The final pH value was adjusted to 1–2 by the addition of aqueous ammonia (NH_4OH). The mixtures were vigorously stirred for 12 h at 70 °C. The resulting white precipitates were washed using ethanol and distilled water, and centrifuged at 8000 rpm. This process was repeated several times, and then dried overnight at room temperature. A part of the as-synthesized powders were annealed at various temperatures.

The X-ray diffraction (XRD) studies were performed on a Rigaku D/max-2000 X-ray powder diffractometer with a Cu target radiation resource ($\lambda = 1.54078$ Å). The operation voltage and current were fixed at 40 kV and 40 mA, respectively. Infrared spectra of powders were recorded in the range of 600–4000 cm^{-1} on a Fourier transform spectrometer (Perkin-Elmer, Spectrum 1, USA) with a resolution of 1 cm^{-1}. The powders were first mixed with KBr then pressed into a cylindrical die. Thermogravimetric analysis (TGA) of powders coupled with differential thermal analysis (DTA) was performed up to 600 °C at the heating rate of 10 °C/min under nitrogen gas flow (TA instruments, model SDT 2960, USA). The size and shape of samples were examined by the scanning electron microscopy (SEM) utilizing a Hitachi S-4800 scanning electron microscope. Energy-dispersive X-ray spectroscopy (EDS) was obtained from an attached Oxford Link ISIS energy-dispersive spectrometer fixed on a Hitachi S-4800 scanning electron microscope. The excitation spectrum and emission spectrum were measured at room temperature with a Hitachi F-4500 fluorescence spectrometer. In the measurement of the fluorescent dynamics of Eu^{3+}, a 266-nm light generated from a fourth-harmonic generator pumped by a pulsed Nd:YAG laser was used as the excitation source.

3. Results and discussion

Fig. 1 shows the XRD patterns of the as-synthesized sample ($Y_{0.97}PO_4$:$Eu_{0.03} \cdot nH_2O$) and those heat-treated at various temperatures. It is noted that, the as-synthesized sample is well crystalline, and that all of the peaks could be well indexed to the monoclinic $YPO_4 \cdot nH_2O$ with churchite-type structure and space group $I2/a$ (JCPDS File No. 85-1842). As the annealing temperature increases to 200 °C, a new diffraction peak is observed, as marked by a specific symbol in Fig. 1. This means that a new phase is involved in the monoclinic phased $YPO_4 \cdot nH_2O$. Further increasing annealing temperature up to 250 °C, the phase with monoclinic structure has almost totally disappeared, a new phase, all of whose peaks could be well indexed to tetragonal dehydrated YPO_4 with xenotime structure and space group $I4_1/amd$ (JCPDS File No. 84-0335), is observed. This indicates that the phase transition from the hydrated YPO_4 with monoclinic churchite-type structure to the dehydrated YPO_4 with tetragonal xenotime-type structure occurs. With further increase of annealing temperature up to 500 °C, it remains dehydrated YPO_4 with tetragonal xenotime-type structure, but the intensifying and narrowing of diffraction peaks are observed, indicating crystal growth of YPO_4 with temperature. The above results indicate that the $YPO_4 \cdot nH_2O$ phase is metastable, which can commonly not be prepared by high-temperature synthesis route. Metastable phased materials can usually be prepared under mild conditions at a relatively low temperature [12]. Fang et al. [17] have used the hydrothermal method to synthesize the anhydrous YPO_4 with tetragonal xenotime-type structure, but they did not obtain the metastable $YPO_4 \cdot nH_2O$ with monoclinic churchite-type structure. It is probably due to the fact that the hydrothermal synthesis is at higher temperature and at a higher pressure than the solution precipitation

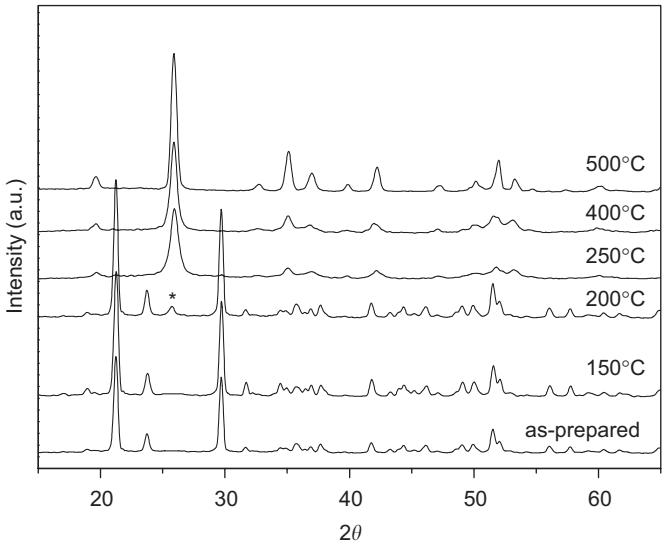

Fig. 1. XRD patterns of the as-synthesized $Y_{0.97}PO_4$:$Eu_{0.03} \cdot nH_2O$ and those annealed at various temperatures for 2 h.

used in this work, which is conducted only at 70 °C and at ambient pressure. This indicates that the structure and composition can be effectively controlled by the synthetic condition and parameters.

Typical TGA and DTA curves of as-synthesized $YPO_4 \cdot nH_2O$ are given in Figs. 2(a) and (b). It can be seen from TGA curve that three steps of weight losses occur in three distinct steps with an overall weight loss of 22% from 40 to 600 °C. The first one occurs in the temperature range 60–150 °C, and is assigned to the release of residual water adsorbed at the powder surface due to the storage in air condition. Accordingly, it corresponds to an endothermic effect in the DTA curve in the temperature range 60–150 °C. The second weight loss (17%) begins at about 150 °C; this corresponds to the dehydration of the hydrated monoclinic YPO_4. Also, a corresponding well-defined endothermic peak is observed in DTA curve in the temperature range 150–350 °C with a sharp peak at 247 °C. This temperature is in good agreement with the phase transition temperature observed in XRD. The third weight loss process is slower up to 600 °C, which is attributed to the decrease or removal of the synthesis residuals and adsorptions such as NO_3^- and OH^-. The weight loss of 17% resulting from the dehydration means about 2 mol water molecules in the $YPO_4 \cdot nH_2O$. The above results indicate that the as-synthesized product undergoes the following thermal equilibrium: $[YPO_4 \cdot nH_2O]_{monoclinic} \rightarrow [YPO_4]_{tetragonal} + nH_2O_{(gas)}$. Certainly, the content of coordinated water can be estimated also by the EDS analysis. The EDS analysis for the as-synthesized sample (Fig. 3) gives an (Y + Eu):P:O atomic ratio of 0.97:1:6.2, which is close to the $YPO_4 \cdot 2H_2O$. This is in almost agreement with the TGA analysis. The EDS analysis for the sample (not shown) annealed at 250 °C gives an (Y + Eu):P:O atomic ratio of 0.98:1:4.05, almost corresponding to the anhydrous YPO_4.

The FTIR spectra of the as-synthesized sample and that annealed at 250 °C are shown in Fig. 4. In the investigated range of wavelength, the characteristic vibrations of phosphate groups are observed: the peak at about 650 cm^{-1} for v_4, the shoulder at 910 cm^{-1} for v_1, and at 1018 and 1060 cm^{-1} for v_3. No other phosphorus-containing groups such as $P_2O_7^{4-}$ (typically located at 1265–1267 cm^{-1}) are observed [18,19], showing that the as-synthesized product has a high purity. For the water vibrations, in addition to the wide bands associated with different types of OH groups, extending from 2700 to 3700 cm^{-1}, the presences of two bands at 1640 and 1715 cm^{-1} and the band at 755 cm^{-1} are indicative of the characteristic of coordinated water molecule [19], i.e., the hydration water molecules in the as-synthesized sample are chemically bonded to the rare earth ions. For the sample annealed at 250 °C, the characteristic vibrations of coordinated water have been completely disappeared due to dehydration at this temperature, which is in good agreement with the EDS result. The band at 1650 cm^{-1} and the band around 3400 cm^{-1} are the

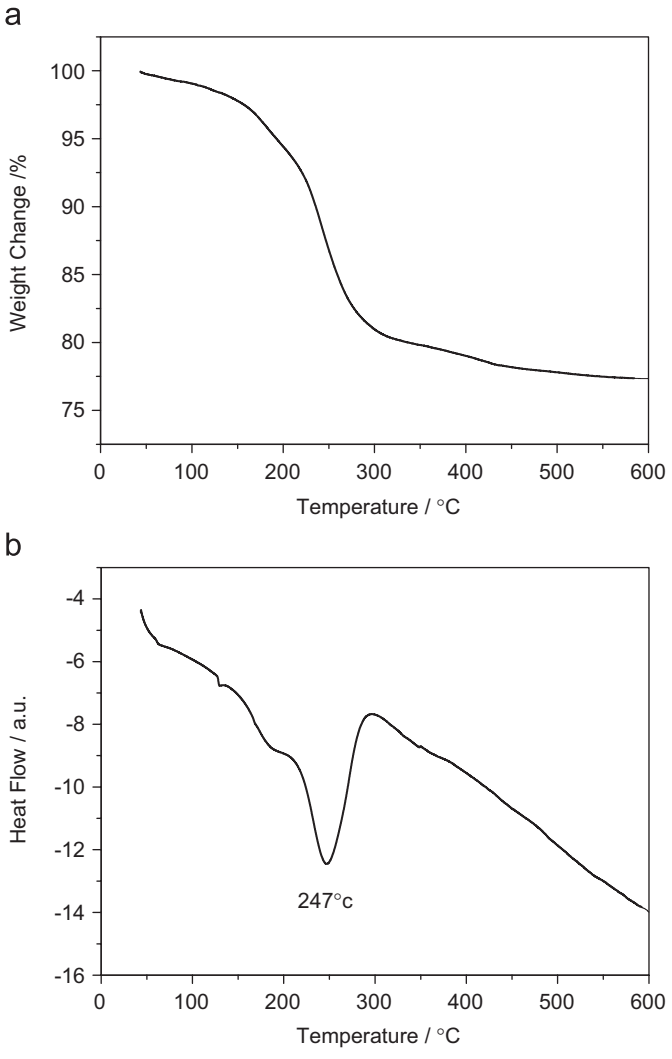

Fig. 2. TGA (a) and DTA (b) plots of the as-synthesized $Y_{0.97}PO_4$:$Eu_{0.03} \cdot nH_2O$.

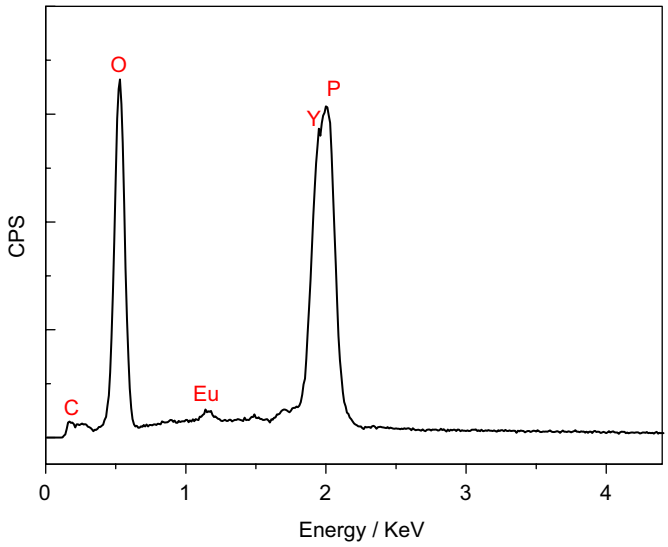

Fig. 3. EDS spectrum of the as-synthesized $Y_{0.97}PO_4$:$Eu_{0.03} \cdot nH_2O$.

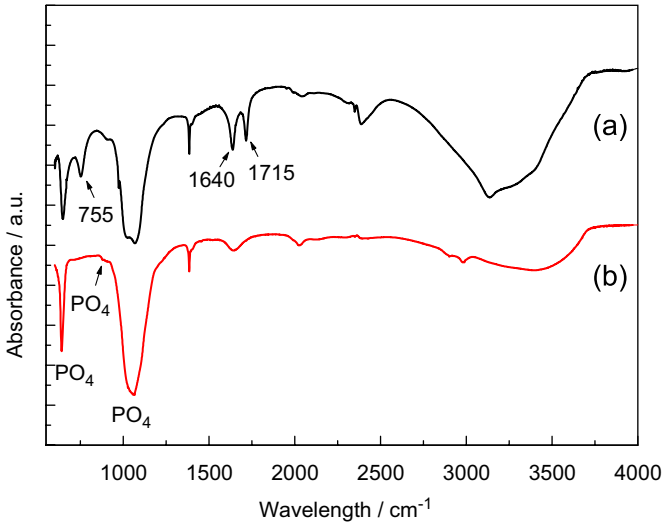

Fig. 4. FTIR spectra of the as-synthesized $Y_{0.97}PO_4:Eu_{0.03}\cdot nH_2O$ (a) and that annealed at 250 °C (b).

characteristic vibrations of water molecules in air physically adsorbed at the sample surface, which is completely different from coordinated water in nature. The band around 1400 cm^{-1} corresponds to the vibration of residual NO_3^- groups [20] originating from the starting reactants ($LnNO_3$). An absorption at 2350 cm^{-1} can be assigned to asymmetric stretching vibration of CO_2 due to the synthesis in air [21]. The above XRD, TGA, DTA, EDS and FTIR analyses show that the as-synthesized products are heavily hydrated due to the presence of coordinated water molecule, and the dehydration at about 250 °C leads to the structural transformation.

The morphology of the as-synthesized samples was examined with field emission scanning electron microscopy (FE-SEM). Typical FE-SEM images of the samples are shown in Fig. 5. The as-synthesized $YPO_4\cdot nH_2O$ samples consist almost entirely of nanowires with diameters of 50–100 nm and a length of about 1–2 μm. These nanowires are distributed densely, indicating a high yield. As the sample was annealed at 250 °C, the structural transition has occurred, but still maintains its original nanowires, and no any increase in size is observed. However, the anhydrous YPO_4 with tetragonal xenotime-type structure synthesized by Fang et al. [17] shows the shape of nanoparticle. They considered that the shape has a strong relation with the crystal structure. The hydrated YPO_4 synthesized in this work shows the crystal structure different from that synthesized by Fang et al. Maybe this is a possible explanation for the formation of nanowires in this work. Lucas et al. used a similar route with us to synthesize the $YPO_4\cdot nH_2O$, and also observed the wire-like shape [10]. The effect of the synthetic condition on the shape can give us an idea for the controlled synthesis: an intermediate phase with a specific structure and morphology is synthesized first, and then transformed to the resulting phase with unaltered shape via a certain transition. A successful example is the conversions of hydroxides into

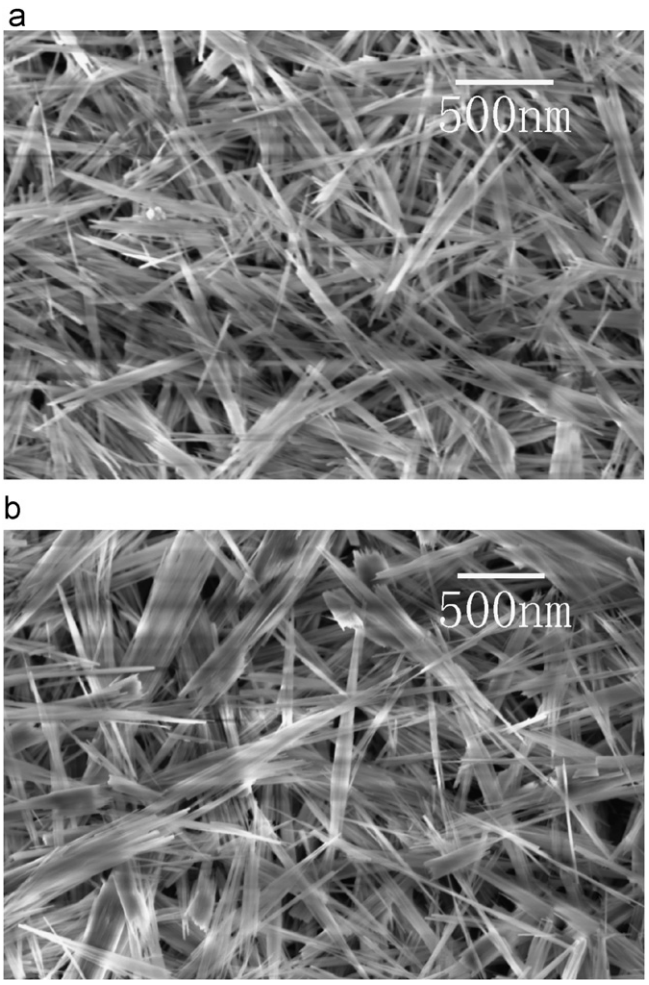

Fig. 5. SEM images of the as-synthesized $Y_{0.97}PO_4:Eu_{0.03}\cdot nH_2O$ (a) and that annealed at 250 °C (b).

oxides, oxyfluorides, and oxysulfides with the same shapes as the as-prepared sample by the dehydration, fluoridation and sulfidation processes, respectively [22]. Similarly, in this work, the metastable YPO_4 hydrates are synthesized first, followed by dehydration to obtain dehydrated YPO_4 with different crystal structure, but still maintain their original shapes.

The excitation spectra of as-synthesized sample and that annealed at 250 °C are shown in Fig. 6. A broad band with a maximum at 235 nm originates from the excitation of the oxygen-to-europium charge transfer band (CTB). The CTB in YPO_4:Eu is highly blue-shift, compared with $LaPO_4$:Eu nanowires available (about 250–260 nm depending on the shape) [17,23,24]. Generally, the peak position of the CTB is dependent on the length of Eu–O bond: the longer the Eu–O bond is, the longer the wavelength of CTB position will be [25,26]. The general *f–f* transitions withn the Eu^{3+} $4f^6$ electron configuration in the longer wavelength region (280–450 nm) can also be observed. These peaks correspond to the direct excitation of the Eu^{3+} ground state into higher levels of the 4f-manifold such as $^7F_0$–$^5L_6$ at 395 nm. For the excitation spectrum of annealed sample, no

significant spectral variation is observed, except for a slight shift of CTB.

Fig. 7 displays the emission spectra of the as-synthesized sample and the sample annealed at 250 °C under 395-nm ($^7F_0$–$^5L_6$) excitation. The spectra consist of sharp lines ranging from 570 to 720 nm, which are associated with the transitions from the excited $^5D_0$ level to ^7F_J ($J = 0, 1, 2, 3, 4$) levels of Eu^{3+} activators. The major emissions around 593 ($^5D_0$–$^7F_1$) and 618 nm ($^5D_0$–$^7F_2$) correspond to orange-red and red color, respectively. Although almost no changes in the spectra shape and position are observed for these two samples that exhibit different crystal structure, the emission intensities present a significant change, i.e., the emission intensity of the sample annealed at 250 °C is about six times as high as that of the as-synthesized sample. For a more detailed comparison, the emission intensities ($^5D_0$–$^7F_1$) of the samples as a function of annealing temperature are given in the inset of this figure. It can be seen clearly that the emission efficiency of the sample annealed at 250 °C shows an abrupt jump; however, those of the samples heat-treated below and above this temperature, 250 °C, have no such significant changes with temperature. The above XRD, TGA, DTA and IR analyses indicated that the as-synthesized samples are heavily hydrated ($YPO_4 \cdot 2H_2O$), in which the hydration water is coordinated to the rare earth ions. While heat-treated at 250 °C, the sample is dehydrated completely, as observed in IR spectra. The removal of coordination water may be a reasonable explanation for a remarkable increase of emission efficiency of the sample annealed at 250 °C. It is well known that hydroxyl groups and water molecule have high vibration frequency ranging from 2700 to 3700 cm^{-1}. The energy separation between $^5D_0$ and $^7F_6$ is about 11,000 cm^{-1}, which may be bridged well by the vibration energy of three water molecules only. Based on the theory of multiphonon relaxation, this makes the $^5D_0$–$^7F_6$ non-radiative relaxation by the bridge of multiphonons highly probable. To support this assumption, the fluorescent decay for $^5D_0$–$^7F_1$ transition of Eu^{3+} was measured and shown in Fig. 8. For the sample annealed at 250 °C, the decay curve at 593 nm shows a nearly single exponential

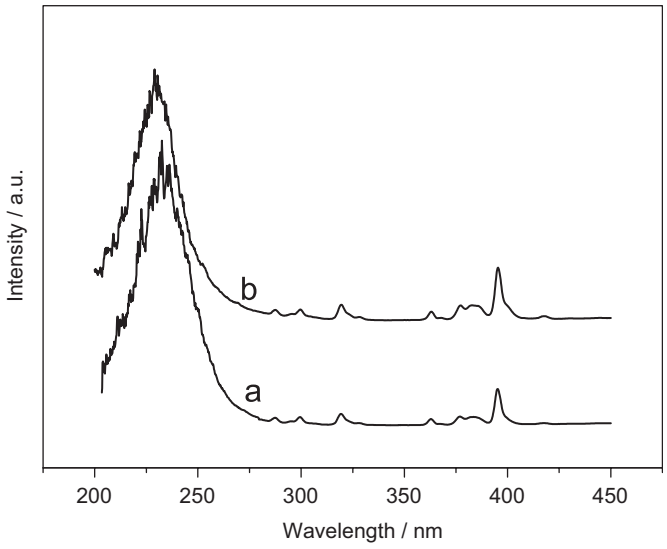

Fig. 6. Excitation spectra of the as-synthesized $Y_{0.97}PO_4$:$Eu_{0.03} \cdot nH_2O$ and that annealed at 250 °C by monitoring the $^5D_0$–$^7F_1$ emission of Eu^{3+}.

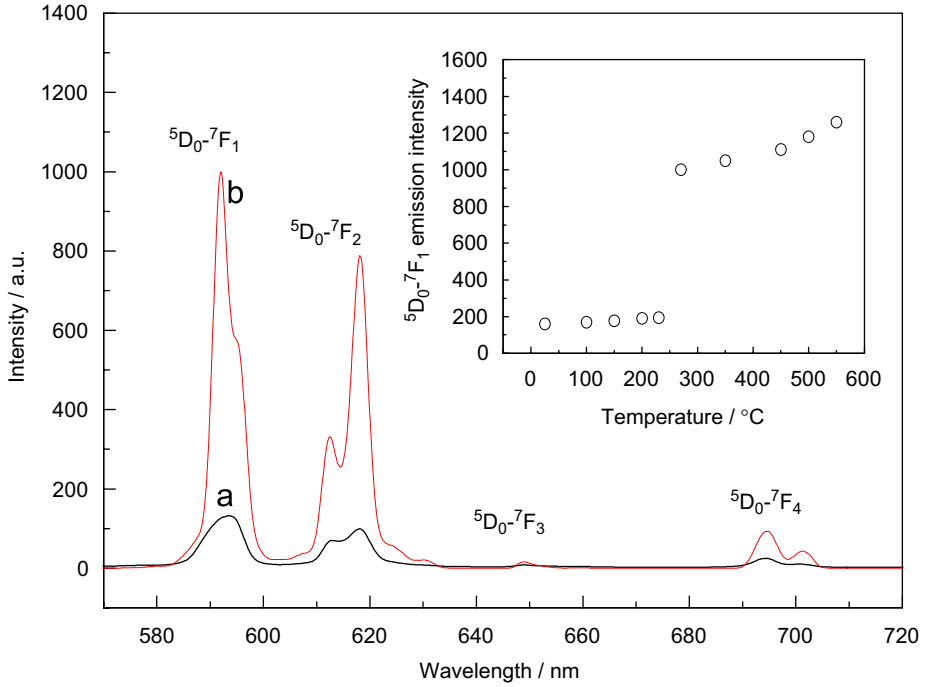

Fig. 7. Emission spectra of the as-synthesized $Y_{0.97}PO_4$:$Eu_{0.03} \cdot nH_2O$ (a) and that annealed at 250 °C (b) under excitation at 395 nm. The $^5D_0$–$^7F_1$ emission intensity as a function of annealing temperature is shown in the inset.

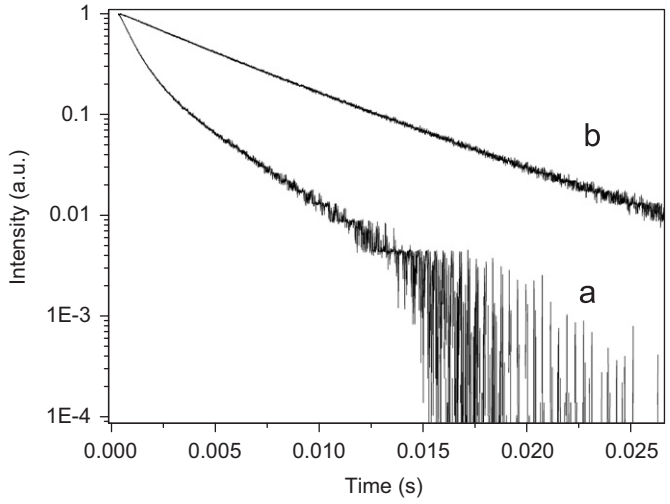

Fig. 8. Fluorescent decay of $^5D_0$–$^7F_1$ of Eu^{3+} in the as-synthesized $Y_{0.97}PO_4$:$Eu_{0.03}\cdot nH_2O$ (a) and that annealed at 250 °C (b).

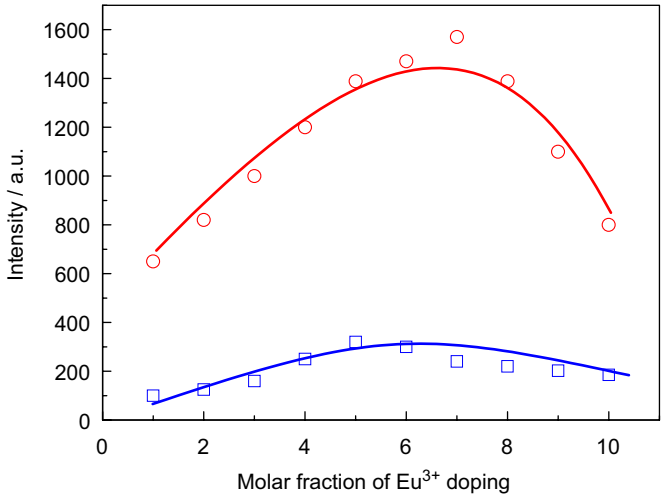

Fig. 9. Quenching concentration of the as-synthesized samples system and corresponding samples system annealed at 250 °C by comparing the emission of $^5D_0$–$^7F_1$.

decay. However, for the as-synthesized sample that contains a certain number of coordinated water, the fluorescent decay deviates from the single exponential behavior, and a fast decay component is observed clearly, which can be explained by the nonradiative relaxation via the high-energy vibration of water molecule. This additional nonradiative energy transfer increases the total relaxation rate of the electrons at the excited states of Eu^{3+} ions, and so explains the drop of the decay time of the emission at 593 nm. Some reports are available on the effect of hydroxyl or water on the luminescent efficiency and lifetime of doped rare earth ions, especially for the luminescent materials with nanometer dimensions [27–30]. In almost all of reported literatures, the mentioned hydroxyl and water affecting the luminescent properties are only surface-adsorbed due to the nature of wet-chemical synthesis. However, in the YPO_4 system investigated in this work, the hydration water is chemically bonded to rare earth ions both at the surface and inside the bulk, and thus a more direct and strong luminescence quenching through nonradiative relaxation should be expected. Therefore, once the coordinated water is removed by annealing at 250 °C, the emission efficiency shows a remarkable increase immediately. Above 250 °C, the emission efficiency only shows a slow increase with temperature. This should be ascribed to the increase of crystallinity and the removal of synthesis residuals such as OH^- and NO_3^-.

Fig. 9 shows the emission intensity ($^5D_0$–$^7F_1$) of Eu^{3+} as a function of Eu^{3+} activator concentration in as-synthesized sample system and a corresponding system annealed at 250 °C. It can be seen that in the as-synthesized system, the effect of activator concentration on the emission efficiency is not as obvious as that in the corresponding system annealed at 250 °C. In addition, the quenching concentration of annealed system shifts to a high one, compared with that of as-synthesized system. The luminescence of doped materials has been well known to related to the concentration of activators and the luminescence killer. The increase of the activator concentration increases the number of luminescent centers, but also enhances the interaction of the excited states. As a consequence, the probability of a nonradiative de-excitation via a luminescence killer is increased, which is called as concentration quenching effect. For the as-synthesized system, a number of coordinated water molecules are present acting as the luminescence killers, so that the number of nonradiative pathways is high enough, and any increase of the mobility of excited state will not significantly modify the emission efficiency. In a corresponding system annealed at 250 °C, in which, the coordinated water are removed completely due to dehydration, the emission efficiency becomes highly sensitive to the activator concentration. In such a system, an optimum activator concentration is 7 mol%, at this level, the maximum emission intensity is observed. Above this concentration, the luminescence decreases with the concentration due to concentration quenching effect. In the as-synthesized samples system, the presence of coordinated water increases the concentration quenching effect significantly, and a lower quenching concentration of about 5% is observed.

4. Conclusions

The Eu^{3+}-doped YPO_4 nanowires have been synthesized by solution precipitation method. XRD, TGA, DTA, EDS and FTIR analyses have indicated that the as-synthesized products are heavily hydrated compound with the monoclinic churchite-type structure, in which the hydration water molecules are coordinated to the rare earth ions. A thermal treatment up to 250 °C results in the dehydration of as-synthesized hydrated sample, also accompanied by the structural transition from the monoclinic churchite-type to the tetragonal xenotime-type. During the thermal

treatment process, the emission efficiency shows a remarkable change, especially for the sample annealed at 250 °C. The emission efficiency of the sample annealed at 250 °C is about six times as high as that of as-synthesized sample. This is attributed primarily to the coordinated water as the nonradiative relaxation pathways in the as-synthesized sample. The FTIR and fluorescent decay dynamics support this conclusion. The activator concentration dependence of the emission efficiency in the as-synthesized samples system is not as sensitive as that in a corresponding samples system that is annealed at 250 °C. The annealed sample system shifts the quenching concentration to a higher value.

Acknowledgments

The authors would like to thank the financial support by National Natural Science Foundation of China (Grant No. 50502031) and the Youth funds of JiLin Province (Grants 20060522).

References

[1] T. Jüstel, H. Nikol, C. Ronda, Angew. Chem. Int. Ed. 41 (1998) 3084.
[2] G. Hebbink, J. Stouwdam, D. Reinhoudt, E. Beggel, Adv. Mater. 14 (2002) 1147.
[3] F. Meiser, C. Cortez, F. Caruso, Angew. Chem. Int. Ed. 43 (2004) 5954.
[4] P. Schuetz, F. Caruso, Chem. Mater. 14 (2002) 4509.
[5] M.Q. Tan, Z.W. Ye, G.L. Wang, J.L. Yuan, Chem. Mater. 16 (2004) 2494.
[6] X. Duan, Y. Huang, Y. Cui, J. Wang, C. Lieber, Nature 409 (2001) 66.
[7] W.B. Bu, Z.L. Hua, H.R. Chen, J.L. Shi, J. Phys. Chem. B 109 (2005) 14461.
[8] X. Wang, Y.D. Li, Chem. Eur. J. 9 (2003) 5627.
[9] O. Lehmann, H. Meyssamy, K. Kompe, H. Schnablegger, M. Haase, J. Phys. Chem. B 107 (2003) 7449.
[10] S. Lucas, E. Champion, D. Bregiroux, D. Bernache-Assollant, F. Audubert, J. Solid State Chem. 177 (2004) 1302.
[11] W.B. Bu, H.R. Chen, Z.L. Hua, Z.C. Liu, W.M. Huang, L.X. Zhang, J.L. Shi, Appl. Phys. Lett. 85 (2004) 4307.
[12] C.J. Jia, L.D. Sun, F. Luo, X.C. Jiang, L.H. Wei, C.H. Yan, Appl. Phys. Lett. 84 (2004) 5305.
[13] W.H. Di, X.J. Wang, B.J. Chen, S.Z. Lu, X.G. Ren, Appl. Phys. Lett. 88 (2006) 011907.
[14] Y.P. Fang, A.W. Xu, A.A.M. Qin, R.J. Yu, Crys. Growth Des. 5 (2005) 1221.
[15] W.H. Di, X.J. Wang, B.J. Chen, S.Z. Lu, X.X. Zhao, J. Phys. Chem. B 109 (2005) 13154.
[16] K. Rajesh, P. Mukundan, P. Krishna Pillai, V.R. Nair, K.G.K. Warrier, Chem. Mater. 16 (2004) 2700.
[17] Y.P. Fang, A.W. Xu, R.Q. Song, H.X. Zhang, L.P. You, J.C. Yu, H.Q. Liu, J. Am. Chem. Soc. 125 (2003) 16025.
[18] C.R. Patra, G. Alexandra, S. Patra, D.S. Jacob, A. Gedanken, A. Landau, Y. Gofer, New J. Chem. 29 (2005) 733.
[19] S. Lucas, E. Champion, D. Bernache-Assollant, G. Leroy, J. Solid State Chem. 177 (2004) 1312.
[20] G.H. Pan, H.W. Song, X. Bai, Z.X. Liu, H.Q. Yu, W.H. Di, S.W. Li, L.B. Fan, X.G. Ren, S.Z. Lu, Chem. Mater. 18 (2006) 4526.
[21] X.C. Wu, Y.R. Tao, C.Y. Song, C.J. Mao, L. Dong, J.J. Zhu, J. Phys. Chem. B 110 (2006) 15791.
[22] X. Wang, Y.D. Li, Chem. Eur. J. 9 (2003) 5627.
[23] H. Meyssamy, K. Riwotzki, A. Kornowski, S. Naused, M. Haase, Adv. Mater. 11 (1999) 840.
[24] V. Buissette, M. Moreau, T. Gacoin, J. Boilot, J. Chane-Chane, T. Mercier, Chem. Mater. 16 (2004) 3767.
[25] Y. Tao, G. Zhao, X. Ju, X. Shao, W. Zhang, S. Xia, Mater. Lett. 28 (1996) 17.
[26] Z.G. Wei, L.D. Sun, C.S. Liao, J.L. Yin, X.C. Jiang, C.H. Yan, J. Phys. Chem. B 106 (2002) 10610.
[27] J.W. Stouwdam, F.C.J.M. van Veggel, Langmuir 20 (2004) 11763.
[28] J.A. Capobianco, F. Vetrone, J.C. Boyer, A. Speghini, M. Bettinelli, Opt. Mater. 19 (2002) 259.
[29] F. Vetrone, J.C. Boyer, J.A. Capobianco, J. Appl. Phys. 96 (2004) 661.
[30] X.C. Jiang, C.H. Yan, L.D. Sun, Z.G. Wei, C.S. Liao, J. Solid State Chem. 175 (2003) 245.